SWEPT FREQUENCY ULTRASONIC IMAGING IN COMPOSITE PLATES

Richard W. Martin
University of Dayton Research Institute
Dayton, Ohio 45469

Dale E. Chimenti
Air Force Materials Laboratory
Wright-Patterson Air Force Base, Ohio 45433

INTRODUCTION

Conventional ultrasonic C-scan imaging normally employs focussed transducers excited by high-voltage impulsive signals. The reflected wave train, containing information about the internal features of the test piece, is translated, either through analog or digital means, to an intensity (or color) and plotted as a function of transducer position on the sample. While this method is certainly effective for many inspections, it is not the only way, or perhaps even the best way, to obtain this kind of information. The purpose of this paper will be to describe an alternate means to acquire ultrasonic C-scan data using a swept-frequency tone-burst imaging technique which presents several important advantages over more conventional means.

This technique has been applied in the standard C-scan geometry to normal incidence reflection waveforms from various types of defects or material discontinuities in fiber-reinforced composites. We use digital signal processing methods to analyze the reflection data and, subsequently, to generate C-scan images which represent defect size, depth, and (x,y) location. The defects in this study consist of impact-generated delaminations in both woven and quasi-isotropic graphite-epoxy plates.

Ultrasonic inspection of composites is a large and active field to which many investigators have contributed over the past dozen years. In addition to an extensive literature on modeling and measurements, much has been written on the application aspects of this problem. While there is not sufficient space here for a full review of the field, recent theoretical contributions have substantially extended appreciation of guided wave behavior in layered plates of anisotropic materials, both in vacuum and immersed in a fluid [1-4]. These calculations have responded to the growing body of experimental results [1,4-6], only a few of which are cited here. Moreover, much applied work has appeared [6-14] on this topic because of its importance to manufacturing quality assurance and in-service NDI.

INSPECTION GEOMETRY

The beam of a focussed (75 mm focal length, 12.5 mm diameter) ultrasonic transducer (8 MHz center frequency) is directed at normal

Review of Progress in Quantitative Nondestructive Evaluation, Vol. 9
Edited by D.O. Thompson and D.E. Chimenti
Plenum Press, New York, 1990

incidence onto the surface of a plate immersed in water. The transducer is excited with a radio frequency (rf) tone-burst whose frequency is swept over the range of about 4 to 12 MHz in 25 milliseconds. The modulation of the rf signal is provided by a 20 Hz triangular waveform which linearly ramps the frequency of the rf generator during each half cycle. Therefore, the rf is essentially constant in frequency over each tone burst, but varies from burst to burst. Tone burst frequency modulation enables us to acquire the test specimen's ultrasonic reflection properties over the full transducer bandwidth. The duration of an individual tone burst (5-30 μsec) is chosen to excite the sample in a quasi-cw fashion (ie. to allow overlap among multiple front and back surface reflections). The resulting constructive and destructive interference of the reflected signal leads to a pattern of peaks and nulls generated in the rf spectrum.

The transducer is operated in the Transmit/Receive mode to acquire the reflected signal from each tone burst. The received signal is amplified, video-detected and filtered. The rf envelope is then sampled and averaged by a boxcar integrator, as shown in Fig. 1, whose aperture is placed in the overlap region of the signal. The output of the integrator is proportional to the signal envelope amplitude and represents the spectral magnitude characteristics of the sample. After filtering to remove any artifacts of the frequency sweep, the signal is sampled with a digitizer at a rate of several kHz. Although the instrument used in this study has a vertical resolution of only 8 bits, at such low sampling rates digitizers capable of much higher resolution could be substituted.

Capturing the rf reflection spectrum as a time domain signal permits further processing to recover a more familiar representation. Results for a 32-ply [0/45/-45/90]s4 quasi-isotropic layup are shown in Fig. 2. The rf amplitude spectrum, indicated as a pseudo time-domain signal, and its 128-point discrete Fourier transform are recorded for a defect-free region of the specimen. The spacing and regularity of the resonances are characteristic of undamaged composite. Its FFT in Fig. 2(b) shows a large peak in a region of the pseudo frequency spectrum we have arbitrarily denoted band #5. This peak near 900 Hz may be taken as indicative of defect-free material. In the data of Fig. 3, acquired over an impact delamination, the pseudo time signal and its transform show the effect of a mechanical discontinuity at about the 8th ply. Many fewer resonances are seen, and the first peak in the pseudo frequency spectrum occurs near 200 Hz.

One important advantage of the swept-frequency tone burst technique is that much greater average acoustic power can be coupled to the test sample than with conventional impulse excitation methods, resulting in a comparatively higher S/N ratio. In fact, acoustic amplitude, expressed as a voltage, is the significant factor determining the signal-to-noise ratio. Making broad assumptions about the experimental conditions, we can estimate the advantage of quasi-cw excitation. Let us take the impulse as triangular and 40 nsec in duration with a maximum height of 500 V. The swept-frequency waveform is 12.5 Vrms and is sampled by the boxcar integrator for an aperture of 10 microsec. Since the transducer characteristics and inspection geometry are identical in each case, the equivalent charge available for signal acquisition is 20 μVsec for each impulse and 125 μVsec for each tone burst. The bursts are repeated at a rate of 2 to 8 kHz. The higher figure substantially improves the rf spectral details in the boxcar output. Each pixel in the method of this paper consists of tone bursts for 25 msec, during which the rf is swept to scan the transducer spectrum.

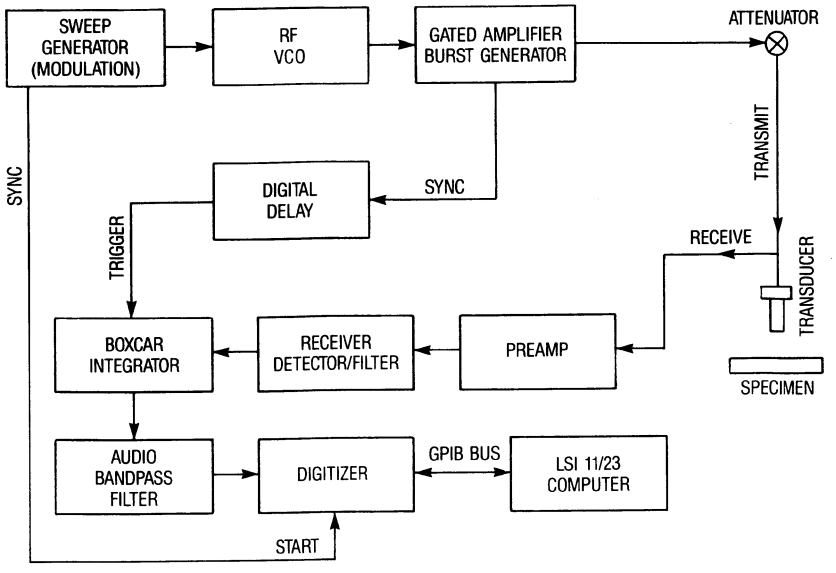

Figure 1. Swept Frequency Tone Burst Instrumentation.

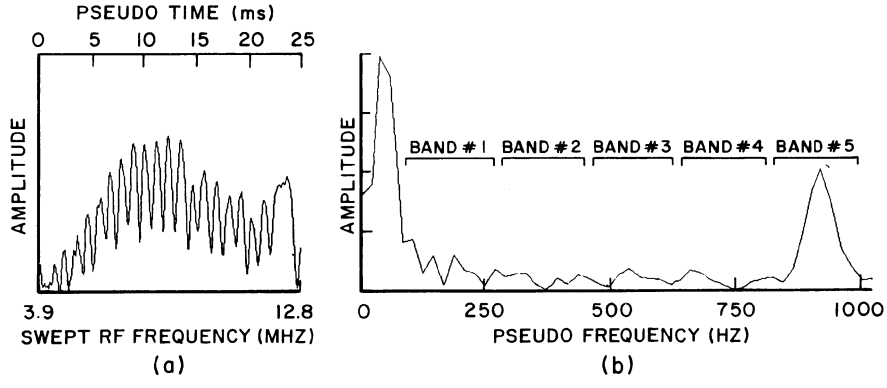

Figure 2. Swept frequency signal amplitudes (a) and corresponding FFT (b) of a defect-free region in a quasi-isotropic composite plate.

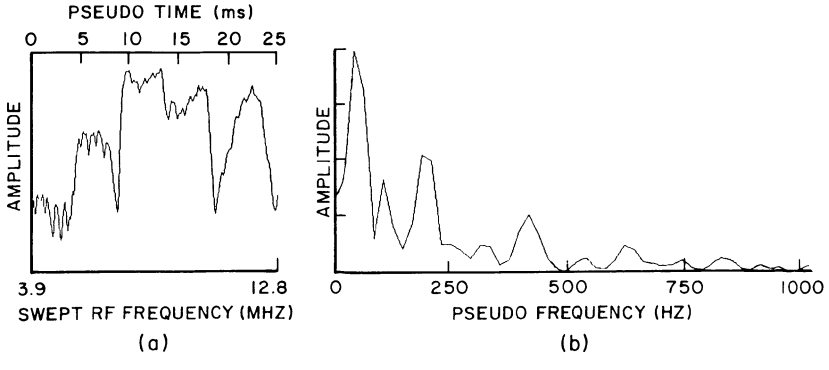

Figure 3. Swept frequency signal amplitudes (a) and corresponding FFT (b) of a delaminated region in a quasi-isotropic composite plate.

Naively, one could compare the total charge ratio for swept-frequency and impulse excitation, (125/20)x(8x25/1) = 1250. This result ignores any averaging which could be done on the impulse signal during the 25 msec frequency sweep. However, instrument limitations prevent either the digital acquisition of such a large amount of data or the rapid transfer of acquired data to computer memory for summation and storage, or both. With readily available instruments, the maximum number of rf time-domain records is about 64, corresponding to 32k channels. At DMA transfer rates using the IEEE-488 protocol, this data would still require at least 200 msec to reach computer memory for accumulation, in addition to the data gathering time. Averaging multiple rf impulses reduces the advantage of the swept-frequency method to a factor of 20, but then slows the impulse scan rate to fewer than five pixels per second. In practice, averaging of rf waveforms is seldom done, because it is complicated, expensive, and time consuming. Moreover, this comparison ignores any nonlinear behavior induced by the large amplitude impulse voltage.

DIGITAL SIGNAL PROCESSING

The envelope of the rf signal is digitized at 5120 samples/sec to obtain 128 data points during the 25 millisecond sweep time (Figs. 2(a) and 3(a)). Then a FFT of the resulting pseudo time signal is computed to determine the pseudo frequency characteristics of the interference pattern. Two methods have been utilized to obtain image data from the FFT magnitude spectrum. Both rely on the shift in frequency of the magnitude spectrum towards lower frequencies in the presence of delaminations. In thick (ie, defect-free) material there are many nulls, as in Fig. 2(a), and the FFT magnitude spectrum indicates this with a large peak near 900 Hz (Fig. 2(b)). In material that is effectively thinner because of mechanical decoupling due to delaminations, there are fewer nulls (Fig. 3(a)). This condition produces a peak which is lower in frequency in the FFT magnitude spectrum (200 Hz and harmonics) and the absence of the peak at 900 Hz (Fig. 3(b)). Herein lies a second important advantage of swept-frequency tone burst imaging. Digitizing at about 5 ksample/sec requires a relatively inexpensive A/D converter compared to the one needed for 50 or 200 Msample/sec capture of a rf time-domain waveform. In addition, kHz sampling rates would permit use of instruments having increased vertical resolution and much higher dynamic range, typically by 24 dB or greater.

The first image generation method employs bandpass filtering techniques which are implemented by integrating the signal within specific bands in the FFT magnitude spectrum. Figure 2(b) shows the location of five frequency bands chosen for this purpose. A peak in band #1 would indicate the presence of a delamination near the entry surface of the specimen and would result in a high value for that filter. Likewise, the presence of delaminations in bands #2, #3 or #4 would indicate respectively deeper delaminations and produce high amplitudes in these filters. The peak in band #5 represents the backsurface of the specimen, so this band will have a large amplitude only for defect-free material. The value of a particular filter at each (x,y) scan point is assigned to a single pixel in a C-scan format. In this manner, C-scan images can be generated for various depths depending upon the filter band selected. Experimental results will be discussed in a later section.

The second image generation method also derives a single value calculated from the pseudo time domain signal, one which characterizes the entire FFT magnitude spectrum at each (x,y) scan point. The median

frequency [8,9] is that frequency which divides the area of the rf magnitude spectrum equally. The median frequency of each (x,y) scan point is mapped to a corresponding pixel, creating a C-scan type image format. Median frequency imaging encodes depth into the grey scale of the image. In defect-free material, the largest number of interference nulls will be observed (assuming constant plate thickness), and the median frequency is consequently high. In material that is effectively thinner because of mechanical decoupling due to delaminations, there are fewer nulls and the median frequency is lower in proportion to the defect's proximity to the sound entry surface. Median frequency spectral processing provides a wide dynamic range of response to defects while preserving sensitivity to small or weak flaws. The defect depth can be estimated and resolved to within the equivalent frequency resolution of the FFT. This outcome and the appearance of Figs. 2(a) and 3(a) are to be expected. Although we have treated the boxcar output in Fig. 1 as a (pseudo) time domain signal, it is nonetheless clearly the rf magnitude spectrum of the plate reflectance. Its FFT will produce a low frequency (slow time) replica of the plate's impulse response. Therefore, the back surface appears at the right-hand side of Fig. 2(b), and a near-surface delamination appears on the left of Fig. 3(b). Results presented in the next section will demonstrate this capability. Median frequency image representation was originally applied to modulated tone-burst leaky Lamb wave generation and is described in previous publications [7-9].

RESULTS

Two graphite-epoxy composite specimens have been investigated in this study. The first specimen is a 32-ply quasi-isotropic (QI) plate with a $[0/+45/-45/90]_{s4}$ layup. The thickness of this sample is 6.85 mm. It contains delaminations caused by a 13.56 joule (10 ft-lb) impact

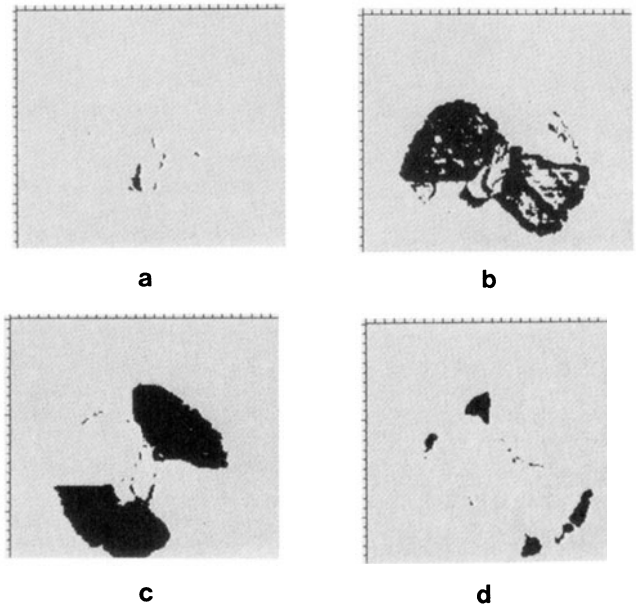

Figure 4. Digital bandpass filtered images of the swept-frequency signal separated into 4 bands. The highest amplitudes in each image are thresholded to black to emphasize the delaminations.

force. The second specimen is a 14-layer woven plate 4.88 mm thick having a simple weave pattern. It has multiple layer delaminations which were induced by an impact force of 2.7 joule (2 ft-lb). Both specimens were subjected to low velocity impacts with a 12.7 mm diameter stainless steel ball on a pendulum impacter to induce delaminations.

C-scan images of delamination damage at 4 different depths in the QI plate were obtained by digital bandpass filtering and are shown in Fig. 4. A 71mm by 71 mm area of this specimen is imaged. Using the frequency bands shown in Fig. 2(b), the image was thresholded into a binary B&W image with the highest amplitudes in each image encoded as black to emphasize the delaminations. We see the typical damage pattern for impacts, where delaminations are oriented in the ply direction at each depth. The area of delamination generally increases with depth [10,11]. Frequency band #1, Fig. 4(a), corresponds to near-surface delamination in a +45 degree ply. Frequency band #2 (Fig. 4(b)) shows delaminations in deeper +45 and 0 degree plies, as does frequency band #3 (Fig. 4(c)) which indicates damage in 90 and -45 degree plies. The deepest delaminations imaged are shown in frequency band #4 (Fig. 4(d)) and are of 0 and +45 degree plies. The depth resolution in these images is about 2 plies, limited by the density of points in the discrete Fourier transform.

The results of applying median frequency (Mfreq) processing to the data from the QI plate are shown in Fig. 5. In this image, Mfreq is encoded as grey scale levels and is proportional to defect depth. White indicates low Mfreq and near-surface delaminations. Light grey through dark grey indicate progressively higher median frequencies and areas of deeper delamination. The highest Mfreq are represented as black in the figure and indicate reflections from the back surface of

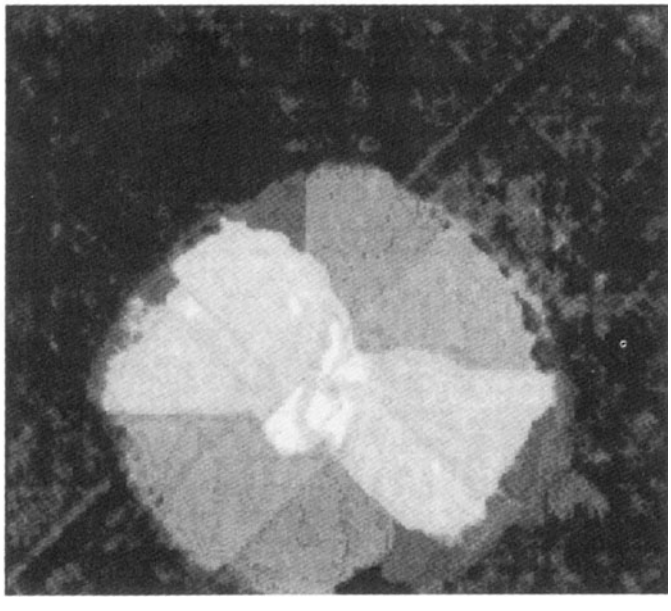

Figure 5. Median-frequency processed image from impacted quasi-isotropic plate. Defect depth encoded as grey scale. White shows near-surface delaminations; black is defect-free material.

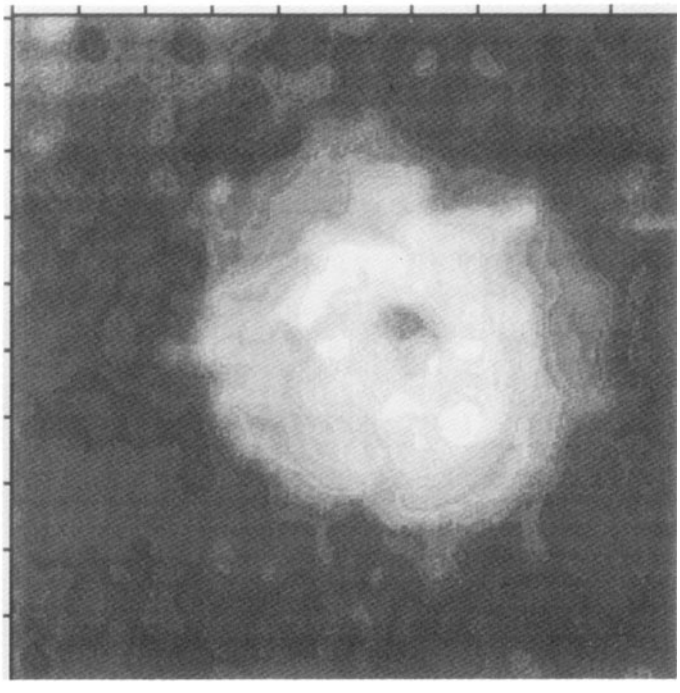

Figure 6. Median frequency processed image of impacted woven plate. Defect depth is encoded as grey scale; white shows near-surface delaminations. Dark grey shows deeper delaminations; black is defect-free material.

the plate (defect-free material). Reflected sound from inhomogeneities in various plies generates linear features along that fiber direction in the image of Fig. 5, indicating the ply layup.

Median frequency processed data from the woven plate is shown in the image of Fig. 6. A 25 mm by 25 mm area of this material has been scanned. The median frequency is encoded as discrete grey scale levels proportional to delamination depth, as in the previous figure. As expected for this type of composite failure mode, increased delamination area with depth is again evident, but with no obvious orientation as in the QI case. The superposition of the weave pattern can be seen on both the delamination and defect-free areas. The impact point can be seen as a grey area near the center of the delamination area. The higher S/N achievable in the swept-frequency tone burst method was essential in obtaining a clear image in this highly attenuative material.

CONCLUSIONS

The relative depths of delaminations and other defects in complex laminates such as woven and quasi-isotropic composites can be determined utilizing swept-frequency techniques and median frequency signal processing. Because many modes are excited, swept-frequency techniques have a high sensitivity to many types of defects at all depths. These techniques are equally applicable to leaky Lamb wave applications. Also, much greater average acoustic amplitude can be

excited in the test sample with quasi-cw swept-frequency techniques than with impulse excitation methods, resulting in a comparatively higher S/N ratio. Lastly, only a low speed (5000 samples/sec) A/D converter is required to digitize the envelope of the rf signal utilizing the described techniques. In addition to being much lower in cost, low speed digitizers usually also offer much greater vertical resolution and dynamic range, which can be of significant value in image enhancement.

ACKNOWLEDGEMENTS

This work was supported under Air Force contract F33615-86-C-5016 and by AFOSR. The authors thank Mr. Mark Ruddell for his assistance in performing the experiments described in this paper.

REFERENCES

1. A. H. Nayfeh and D. E. Chimenti, "Ultrasonic wave reflection from liquid-coupled orthotropic plates with application to fibrous composites", J. Appl. Mech. 55, 863 (1988).
2. S. K. Datta, A. H. Shah, R. L. Bratton, and T. Chakraborty, "Wave propagation in laminated composite plates", J. Acoust. Soc. Am. 83, 2020 (1988).
3. Y. Li and R. B. Thompson, "Propagation of guided waves in orthotropic plates", in Review of Progres in QNDE, Vol. 8A, eds. D. O. Thompson and D. E. Chimenti, (Plenum Press, New York, 1989), p. 189.
4. A. K. Mal and Y. Bar-Cohen, "Ultrasonic characterization of composite laminates", Wave Propagation in Structural Composites, (ASME, New York, 1988) AMD-Vol 90, p. 1.
5. D. E. Chimenti and A. H. Nayfeh, "Ultrasonic Reflection and Wave Propagation in Multilayered Composite Plates", in Review of Progress in QNDE, Vol. 8A, eds. D. O. Thompson and D. E. Chimenti, (Plenum Press, New York, 1989), p. 221.
6. P. B. Nagy, L. Adler, D. Mih, and W. Shephard, "Single mode Lamb wave inspection of composite laminates", in Review of Progress in QNDE, op. cit., Vol. 8B, (1989) p. 1535.
7. D. E. Chimenti and Y. Bar-Cohen, "Signal analysis of leaky Lamb wave spectra for NDE of composites", in Proceedings of 1985 IEEE Ultrasonics Symposium, ed. B. R. McAvoy, (IEEE, New York, 1986) p. 1028.
8. R. W. Martin and D. E. Chimenti, "Signal Processing of Leaky Lamb Wave Data for Defect Imaging in Composite Laminates," in Review of Progress in QNDE, op. cit., Vol. 6A, (1987) p. 815.
9. R. W. Martin and D. E. Chimenti,"Leaky Plate Wave Inspection of Biaxial Composites", Review of Progress in QNDE, op. cit., Vol 8B, (1989) p 1663.
10. B. G. Frock, R. W. Martin, T. J. Moran, and K. O. Shimmin, "Imaging of Impact Damage in Composite Materials", Review Of Progress in QNDE, op. cit., Vol 7B, (1988) p.1093.
11. C. F. Buynak, T. W. Moran and R. W. Martin, "Delamination and Crack Imaging in Graphite/Epoxy Composites," Materials Eval. 47, 438 (1989).
12. L. H. Pearson and W. J. Murri, in Review of Progress in QNDE, op. cit., Vol. 5B, (1986) p. 1093.
13. W. R. Rose, S. I. Rokhlin, and L. Adler, in Review of Progress in QNDE, op. cit., Vol. 5B, (1986) p. 1111.
14. Y. Bar-Cohen and D. E. Chimenti, "Nondestructive evaluation of composites by leaky Lamb waves", in Review of Progress in QNDE, op. cit., Vol. 5B, (1986) p. 1199.